

Photocatalytic and Antimicrobial Properties of [AgTiO₂]:[Clay] Nanocomposite Prepared with Clay Different Ratios

Lemeyonuin Aliou Guillaume Pohan^{1,2*}, Ollo Kambiré³, Muhammad Nasir^{2*}, Lassiné Ouattara⁴

¹UFR Sciences Biologiques, Université Peleforo Gon Coulibaly de Korhogo, Korhogo, Côte d'Ivoire

²Interdisciplinary Research Centre in Biomedical Materials, COMSAT University Islamabad-Lahore Campus (CUI), Lahore, Pakistan

³UFR Sciences et Technologies, Université de Man, Man, Côte d'Ivoire

⁴Laboratoire de Constitution et réaction de la matière, UFR SSMT, Université Félix Houphouët-Boigny de Cocody, Abidjan, Côte d'Ivoire

Email: *pohan.aliou@gmail.com, *muhammadnasir@cuilahore.edu.pk

How to cite this paper: Pohan, L.A.G., Kambiré, O., Nasir, M. and Ouattara, L. (2020) Photocatalytic and Antimicrobial Properties of [AgTiO₂]:[Clay] Nanocomposite Prepared with Clay Different Ratios. *Modern Research in Catalysis*, 9, 47-61.

<https://doi.org/10.4236/mrc.2020.94004>

Received: September 24, 2020

Accepted: October 27, 2020

Published: October 30, 2020

Copyright © 2020 by author(s) and Scientific Research Publishing Inc.

This work is licensed under the Creative Commons Attribution International License (CC BY 4.0).

<http://creativecommons.org/licenses/by/4.0/>



Open Access

Abstract

This work aimed to synthesis a novel material that would be able to efficiently remove both organic and microbiological pollutants from wastewater. Through the hydrothermal process, we first doped titanium dioxide, a semiconductor possessing excellent photocatalytic properties with silver nanoparticles having good antibacterial properties. The obtained material was then associated with clay known for its good adsorbent properties to form [Ag-TiO₂]:[clay] type nanocomposites. The different mass composition of [Ag-TiO₂]:[clay] considered in this work were 1:1; 1:0.5; 1:0.1; 1:0.05 and 1:0.01. The prepared nanocomposites were characterized by means of XRD, FTIR and SEM techniques. Results revealed the presence of TiO₂ anatase and Ag on the surface of the clay mainly composed of kaolinite and quartz. The photocatalytic activities of the nanocomposites were tested in the presence of synthetic Orange II (25 mg/L) wastewater under visible light irradiation. The experiments demonstrated that organic pollutants were effectively photodegraded when the proportion of clay in the mixture (AgTiO₂)-(Clay) was inferior or equaled to 50%. The use of commercial TiO₂, for comparison purpose, showed a lower degradation efficiency of the Orange II solution ($\eta < 30\%$). The antibacterial properties of the nanocomposites [AgTiO₂]:[clay] were also assessed in the presence of two types of bacteria *E. coli* (Gram negative) and *S. aureus* (Gram positive). The antibacterial activities of the nanocomposites were characterized with and without UV irradiation. In dark conditions, the antibacterial activities of nanocomposites (AgTiO₂)-(Clay) against *S. aureus* gradually increased with increasing the clay amount. Under visible light ir-

radiation, the nanocomposites showed a significant antimicrobial activity against *E. coli* and *S. aureus*.

Keywords

Photocatalysis, Antimicrobial Activity, Organic Pollutant, Clay, Wastewater

1. Introduction

According to the World Health Organization, contaminated water contributes to the transmission of infectious diseases. Among those we should cite diarrhea, cholera, dysentery, typhoid, and polio. Besides, contaminated water has severe impacts on prevalence and risk of malnutrition [1]. The major pathogens agents responsible for these diseases are *Staphylococcus aureus*, *Enterococcus*, *Klebsiella pneumoniae* and *Escherichia coli* [2] [3] [4]. In Africa, about 115 people die every hour due to the utilization of contaminated waters by microorganisms or organic pollutants [5]. The conventional biological treatment processes are limited for removal persistent organic pollutants. Adsorption and coagulation-flocculation methods are not efficient for removal all types of organic pollutants and reducing pathogens agents [6]. Heterogenous photocatalysis as an effective technique has received great attention for the purification of polluted water [7] [8] [9]. This technique is considered to be environmentally friendly. Photocatalysis is based upon the use of UV irradiated semiconductor catalysts. Thus, the efficient treatment of contaminated waters can be achieved by modifying the surface of photocatalysts with the introduction of metal nanoparticles having antibacterial properties [10].

Metallic nanoparticles (NPs) such as gold, copper, zinc, titanium, silver (Ag) have received great attention due to their unique physical and chemical properties [11] [12]. Ag NPs possess good bactericidal properties against wide selection of microorganisms including bacteria, fungi and virus [13]. However, Ag NPs applications for wastewater treatment are limited by its strong tendency to form aggregates [14]. Using supports is one of the attractive techniques to stabilize Ag nanoparticles [15] [16].

The clays are widely used as support due to their high specific surface area, chemical and mechanical stability, structural properties and low cost. Also, doping TiO₂ with Ag NPs is one of the common methods applied to increase the photocatalytic activity of TiO₂ under visible light and sun lights [17] [18]. The enhancement is attributed to its ability to trap electrons at Schottky barriers at each Ag-TiO₂ contact region, which reduces the recombination of light generated electrons and holes (e⁻ and h⁺) at the TiO₂ surface. Therefore, charge separation is promoted, and more electron transfer occurs, inducing longer electron-hole pair lifetimes [19].

The main objective of this work consisted in developing AgTiO₂/clay nanocomposites that would be able to efficiently remove both organic and microbio-

logical pollutants from wastewater. Owing its high specific surface area, using clay in the system was expected to improve the absorption and adsorption properties of the prepared nanocomposite. Different proportions of clay from Côte d'Ivoire, in association with Ag-doped TiO₂ NPs were considered. And the photocatalytic and antimicrobial properties of the obtained AgTiO₂/clay nanocomposite were characterized.

2. Experimental Procedure

2.1. Materials

The clay material used in this work was collected from the Hambol region (Katiola, North of Côte d'Ivoire). All major reagents utilized for synthesis were AR grade and were used as-received. Titanium sulfate provided by Bodi Chemical co. and silver nitrate supplied by Sigma-Aldrich were used as titanium and silver sources respectively. Orange II purchased from Eyer was used to assess the degradation performance of the samples. Double distilled water was used throughout the experiment. *S. aureus* (ATCC 6538) and *E. coli* (ATCC) were obtained from local suppliers.

2.2. Synthesis of the Nanocomposites

The nanocomposites were prepared through a simple hydrothermal method using titanium sulfate and silver nitrate as precursor materials for Ti and Ag respectively, and clay. Before using, the clay was crushed, washed and activated in line with the procedure described by Guillaume *et al.* [20]. 5 g of titanium sulfate and 0.11 g of silver nitrate were dissolved in 150 mL of ultra-pure water. The mixture was kept in a dark room at ambient temperature under constant stirring to enable the complete dissolution of reactants. Various amounts of clay (*i.e.* 0.05, 0.25, 0.5, 2.5, and 5 g) were then added to the reaction mixture still under strong stirring for 2 hours. Afterwards, the ensemble was placed in an oven at 150°C for 24 hours to undergo the hydrothermal treatment. The obtained products were ground and calcined in a furnace at 450°C for 2 hours.

2.3. Characterization Techniques

The structural properties of the specimens were determined by means of X-ray diffractometer (XRD, Rigaku D/MAX 2550, Cu K α radiation, $\lambda = 1.5406 \text{ \AA}$) set at 40 kV and 100 - 200 mA in the range of 20° - 80° (2 θ). The sample morphologies were characterized using Scanning electron microscope (SEM, Tescan VEGA3). FTIR spectra were recorded in the 400 - 4000 cm⁻¹ range with NICOLET 380 FTIR spectrometer. Experiments were performed on prepared KBr/sample pellets.

2.4. Photocatalysis Experiments

The photocatalytic activity efficiencies of the prepared samples were evaluated by degradation of 25 mg/L solution of Orange II. The photocatalytic activity

tests were carried out under ambient temperature in a homemade photocatalytic reactor consisting of 500 W tungsten halogen lamp, put in a double wall jacketed quartz cylinder. Cold water was circulated through the walls for lowering the lamp temperature. A glass filter was inserted between the lamp and the sample to filter out UV light ($k < 420$ nm). Also, two fans were attached to the reactor; one was directly linked to the lamp while the other was used to cool the catalyst pollutant suspensions. The distance maintained between the lamp and the center of the quartz tube was 10 cm. Degradation studies were performed with 25 mg/L Orange II dye for a period time of 3 hours. 0.1 g of the catalyst was added to 50 mL of dye solution. Before irradiation of light, the samples were kept in dark under stirring to help the adsorption of samples on the surface of dye molecules. Sampling was performed hourly and centrifuged. Then degradation was evaluated by means of UV visible spectrometer (Shimadzu UV-2450). The adsorption/photodegradation efficiency of dyes was calculated using the following relation (1):

$$\eta = \frac{C_0 - C_t}{C_0} \times 100 \quad (1)$$

where C_0 represents the initial concentration of the pollutants and C_t the concentration of the pollutants at time t .

2.5. Antibacterial activity

For antibacterial experiment, *E. coli* (gram negative) and *S. aureus* (gram positive) bacteria were used as the target organisms. Luria Bertani (LB) broth and Muller Hinton (MH) agar were used for the growth of selected bacterium. Prior to the experimentation, each material and equipment was submitted to an autoclave sterilization. In the liquid culture the bacterial density was measured by its Optical density by means of UV-Vis Spectrophotometer at the wavelength of 600 nm and OD values were taken equal to 0.2. A 200 - 300 μ L aliquot of the liquid culture was used for bacterial growth on agar plates, containing 105 colony-forming units (CFU). The antibacterial activity of the samples was observed using disk diffusion assay.

The aliquot containing bacteria were streaked evenly on the MH agar plates using sterilized cotton swabs. After drying the plates for 5 - 10 minutes, 10 mm diameter of sterilized samples were placed on the plate along with the positive control *i.e.* Amikacin disks for *S. aureus* and sulphamethaxazole for *E. coli*. After 24 hours of incubation at 37°C in the incubator, the inhibition zones were measured.

3. Results and Discussion

3.1. Characterization of Prepared Nanocomposites

SEM images of the clay, titanium oxide, silver doped TiO₂ and silver doped TiO₂ with clay composites are shown in **Figure 1**. SEM image of TiO₂ shows surface compactness and some clustered nanoparticles and no cracks was found during

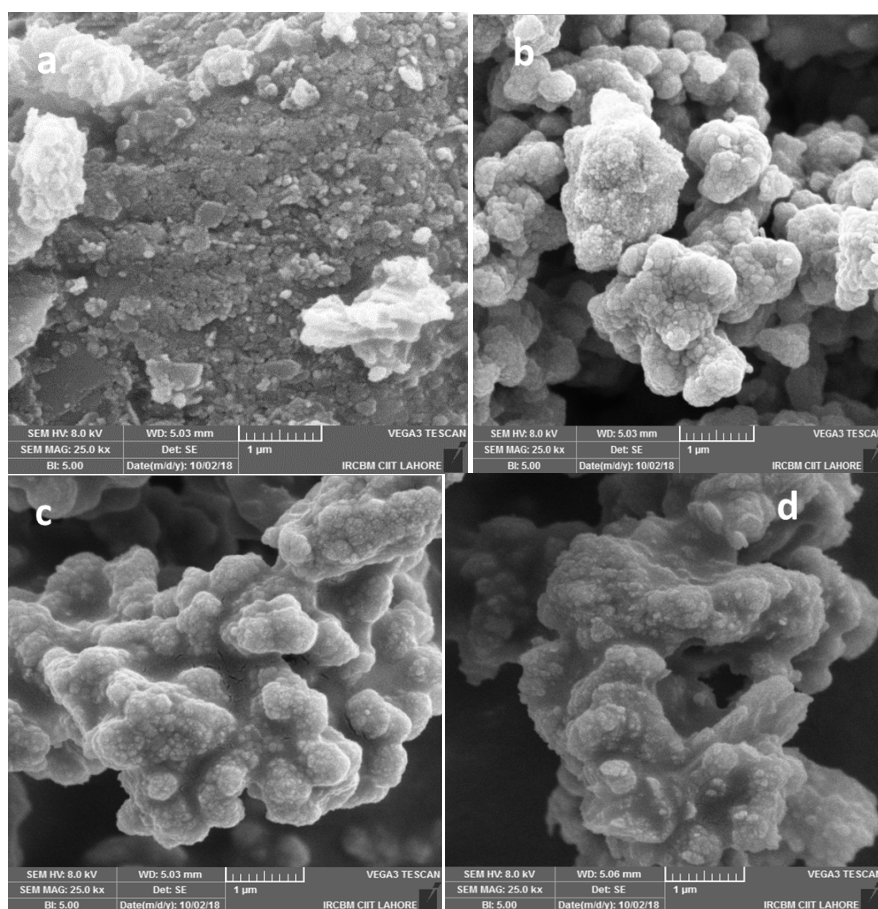


Figure 1. Microstructural observations of specimens: (a) Clay, (b) TiO₂, (c) Ag-TiO₂ and (d) Clay: Ag-TiO₂.

annealing process at 450°C. The incorporation of Ag in TiO₂ nanoparticles induces a change in the structure with respect to the one of the non-doped TiO₂. Ag nanoparticles form micron-sized aggregates on the surface of TiO₂ with a non-uniform distribution. The particles present in the silver doped TiO₂ appear smaller than those of the non-doped TiO₂. A more compact material with a cementation like phenomenon is observed suggesting an increase in the reactivity of the material. Also, one can observe the presence of cracks on the surface of Ag-doped TiO₂ specimen. Besides, adding clay in the Ag-doped TiO₂ system further improves the microstructure of the material with high roughness. However, cracks are still present on the surface of the material. The small size of particles and the fissures along with clay sheets could improve effectively the pollutant absorption and photocatalytic applications [19].

Figure 2 shows the FTIR spectra of the prepared Ag doped TiO₂ mixed with various amount of clay. Peaks around 3500 cm⁻¹ and 2400 cm⁻¹ are related to the stretching vibration of OH groups (Ti-OH) in the TiO₂ samples [20] [21]. Increasing the clay content in the system enables an increase in OH groups. This is quite beneficial for the photocatalysis, as it attracts more pollutants on the surface of the samples. A set of bands located from 900 cm⁻¹ to 1100 cm⁻¹ seems to

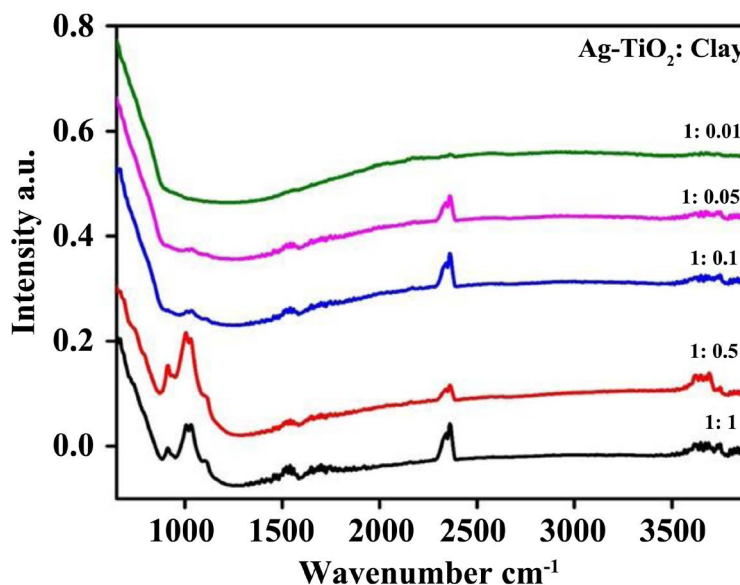


Figure 2. FTIR of prepared silver doped TiO₂ nanoparticles and their composites with different ratios.

be linked to the presence of the clay. As, these bands which clearly appear in the case of high amount of clay (Ag-TiO₂: clay corresponding to 1:1 and 1:0.5), are quasi-absent when the clay content is very low. The band that appears at 914 cm⁻¹ is associated with the vibration of hydroxyls groups of aluminum surface (Al-OH). The band located around 1019 cm⁻¹ is related to the stretching vibration of Si-O-Si bonds. Whereas the one 1112 cm⁻¹ is corresponded to the stretching vibration of Si-O bonds [22]. The FTIR band at 1500 cm⁻¹ could be assigned to the interaction between Ag and TiO₂ particles [23].

The X-ray diffraction patterns of clay and the prepared [AgTiO₂]:[clay] samples are shown in Figure 3. The [AgTiO₂]:[clay] pattern shows the presence of phases related to the initial constituent elements (*i.e.* Ag, TiO₂ and clay). The TiO₂ detected is anatase phase with the mains peaks at 25.65° and 54.41° corresponding to the [1 0 1] and [1 0 5] crystal planes respectively [20] [24] [25]. Therefore, there were no rutile and brookite phases [26] [27]. Silver (Ag) peaks corresponding to [1 1 1], [2 0 0], and [2 2 0] reflections appear at 38.08°, 48.43° and 63.07°. Also, the peaks of kaolinite (Al₂Si₂O₅(OH)₄) and quartz (SiO₂) are observed at 35.23° and 36.68°, respectively due to the presence of clay.

3.2. Photocatalytic Studies of Prepared Nanocomposites

The photocatalytic efficiencies of the prepared nanocomposites were evaluated by degradation of 25 mg/L solution of Orange II under visible irradiation. The experimental results for the degradation of Orange II are given in Figure 4(a) and Figure 4(b) for commercial TiO₂, Ag doped TiO₂ and [AgTiO₂]:[clay] with different ratios of clay. The commercial TiO₂ which is a standard photocatalyst was used as the reference to compare its photodegradation activity for dye with the one of AgTiO₂ and [AgTiO₂]:[clay] samples. In fact, this comparison is

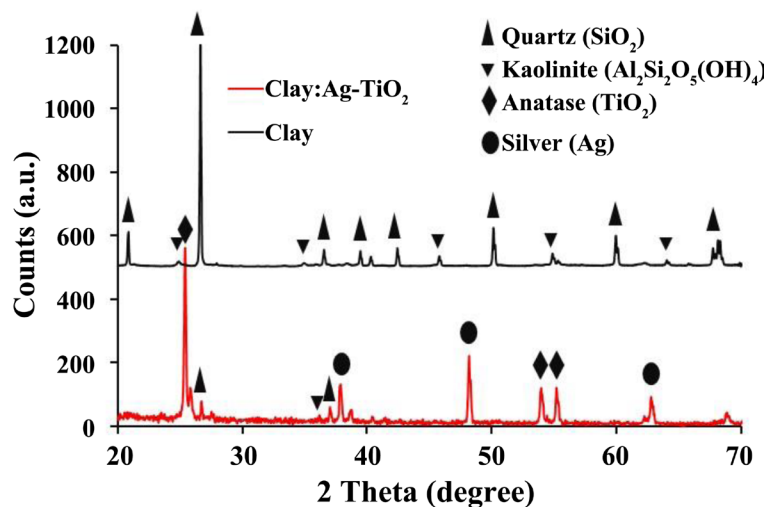
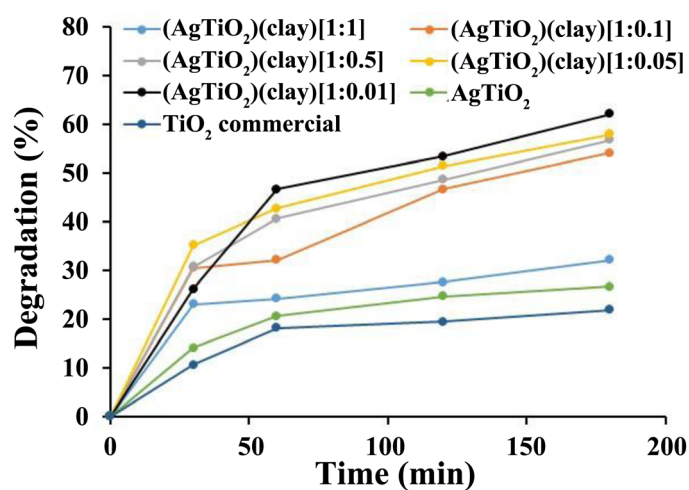
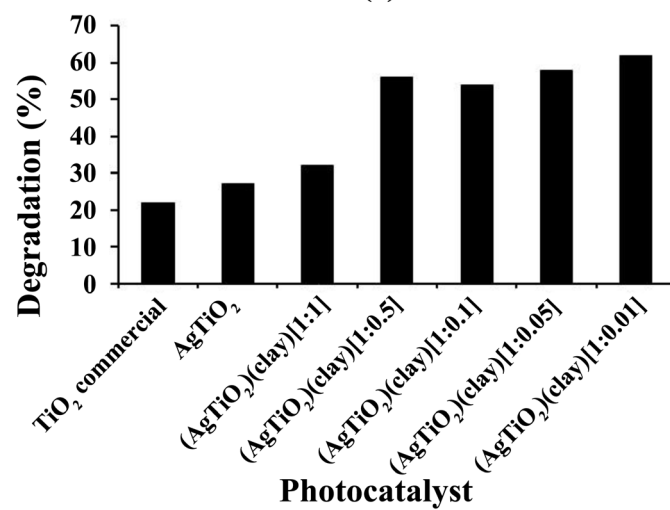


Figure 3. XRD patterns of clay and the prepared Ag-TiO₂:Clay nanocomposite.



(a)



(b)

Figure 4. Efficiency for photocatalytic degradation. (a) Degradation of Orange II versus time (min) over clay/TiO₂-Ag, (b) Degradation versus photocatalysts used, after 180 min.

necessary to evaluate the synergic effect of the prepared nanocomposites. **Figure 4(a)** shows that composites of clay and silver doped TiO₂ nanoparticles exhibit better photocatalytic activity than that of the commercial TiO₂ nanoparticles. The good performance of the prepared nanocomposite is due to the combined effect of the silver and the clay. Clay provides better adsorption characteristics to the nanoparticles whereas silver helps to increase the electrical properties of the samples. Furthermore, findings showed that the increase in the clay content in the system induces a decline in the sample activity. This could be due to the coating of TiO₂ nanoparticles by clay. This coating of TiO₂ NPs could be blocking them from exposure to the dye molecules and hence stopping them from doing their action. Degradation pattern of nanoparticles could be better evaluated from **Figure 4(b)** as well where we showed the percentage degradation of each composite as compared to the TiO₂ nanoparticles. For commercial TiO₂, 22% of Orange II were removed after 180 min of irradiation. When we have doped TiO₂ with Ag, the removal efficiency increase is from 22% to 27%. When Ag doped TiO₂ is associated to clay, the removal efficiency increase from 27% to 32%, 54%, 57%, 58%, and 62% for 5, 0.5, 2.5, 0.25 and 0.05 g amounts of clay added, respectively.

3.3. Kinetic Study

Kinetics study of the photocatalytic degradation of 25 mg/L solution of Orange II is described using the pseudo-first-order model (**Figure 5**): $\ln\left(\frac{C_0}{C_t}\right) = kt$;

where C_0 and C_t are the concentrations of dye in the solution at time 0 and t (min), respectively, k is the rate constant (min^{-1}). The results of rate constant and R^2 are displayed in **Table 1**. These results reveal that the rate constant for TiO₂ commercial increase to 19% with incorporation of Ag in the photocatalyst.

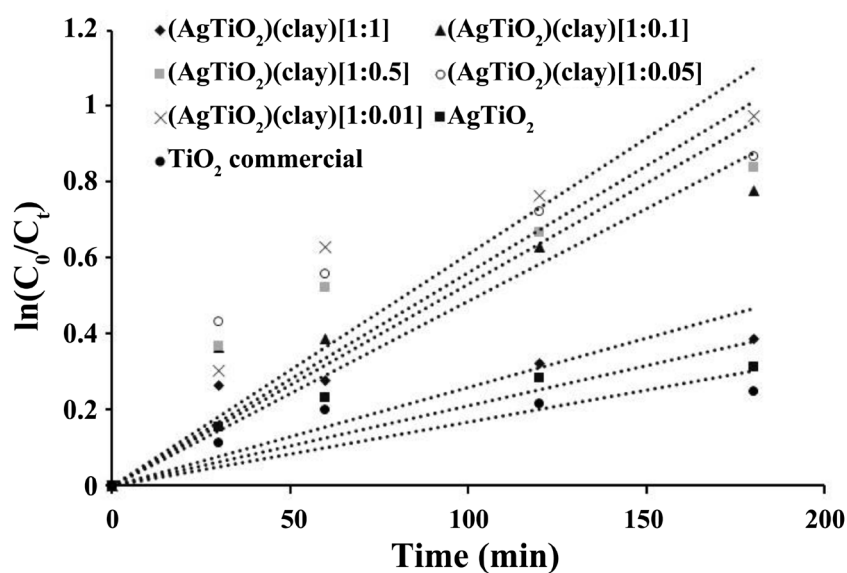


Figure 5. Kinetic of degradation of Orange II with different nanocomposites.

Table 1. Photodegradation kinetics parameters of Orange II with different nanocomposites.

Materials	k (min ⁻¹)	R ²
TiO ₂	0.0017	0.5756
AgTiO ₂	0.0021	0.6079
(AgTiO ₂)(clay)[1:1]	0.0026	0.3685
(AgTiO ₂)(clay)[1:0.5]	0.0053	0.7571
(AgTiO ₂)(clay)[1:0.1]	0.0049	0.8065
(AgTiO ₂)(clay)[1:0.05]	0.0056	0.6782
(AgTiO ₂)(clay)[1:0.01]	0.0061	0.8304

This observation could be attributed to the reduction of recombination of electron and holes. **Table 1** shows that the AgTiO₂/clay have rate constant which is higher than the Ag doped titanium oxide. This is due to the synergic effect between adsorption and photoactivity. The presence of clay increases the surface area of the nanocomposite that offers more sites for the dye to adsorb and hence degrade. However, the rate constant decrease when the amount of clay is important. The (AgTiO₂)(clay)[1:1] sample displayed rate constant 2.34 times lower than (AgTiO₂)(clay)[1:0.01]. The slow rate constant might be due to the reduction of hydroxide radical production resultant to the react of TiO₂ and the photons. Thus, the large amount of clay prevents TiO₂ to products hydroxyl radicals necessary for the dye degradation.

3.4. Antimicrobial Activity of Prepared Nanocomposites

For antimicrobial activity, we named the nanocomposites 18, 19, 20, 21, 22 and 23. 18 is silver doped TiO₂ and clay nanocomposite with ratio 1:1, 19 is silver doped TiO₂ and clay nanocomposite with ratio 1:0.5, 20 is silver doped TiO₂ and clay nanocomposite with ratio 1:0.1, 21 is silver doped TiO₂ and clay nanocomposite with ratio 1:0.05, 22 is silver doped TiO₂ and clay nanocomposite with ratio 1:0.01, 23 is silver doped TiO₂ nanoparticles.

3.4.1. Activity in Dark

In the dark the intrinsic activity of the nanocomposites was evaluated. **Figure 6** and **Figure 7** shows the disk diffusion bactericidal photographs for gram-positive bacteria (*S. aureus*) and gram-negative (*E. coli*), respectively. Against gram-positive bacteria *S. aureus* (**Figure 6**, SA 2 in the petri dish is control antibiotic), inhibition zones were observed with prepared nanocomposites. These observations suggest that clay and Ag NPs contribute very well to antimicrobial activity in AgTiO₂/Clay structures. Thus, in dark *S. aureus* could have a good adsorption on clay and react with Ag NPs deposited to TiO₂. In fact, the Ag atoms were in direct contact with the TiO₂ nanoparticles. The radius of the Ag⁺ and Ag atom is much larger than the Ti⁴⁺, so very unlikely for Ag⁺ and Ag atom to enter the TiO₂ lattice [28].

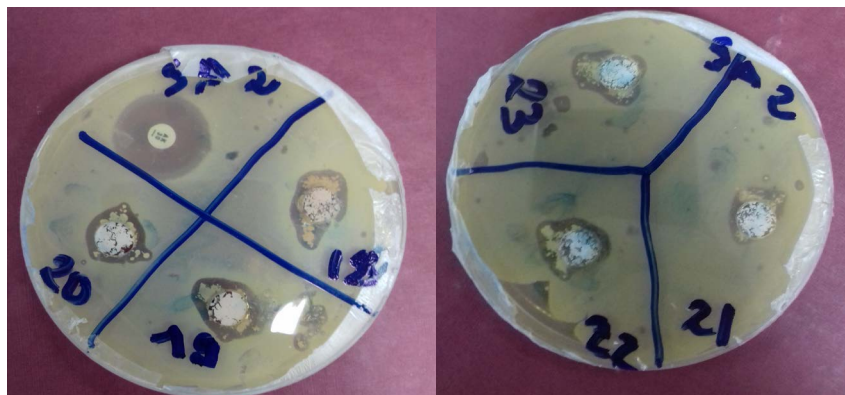


Figure 6. Antimicrobial activity of nanocomposites with *S. aureus* bacterial strains, in dark.

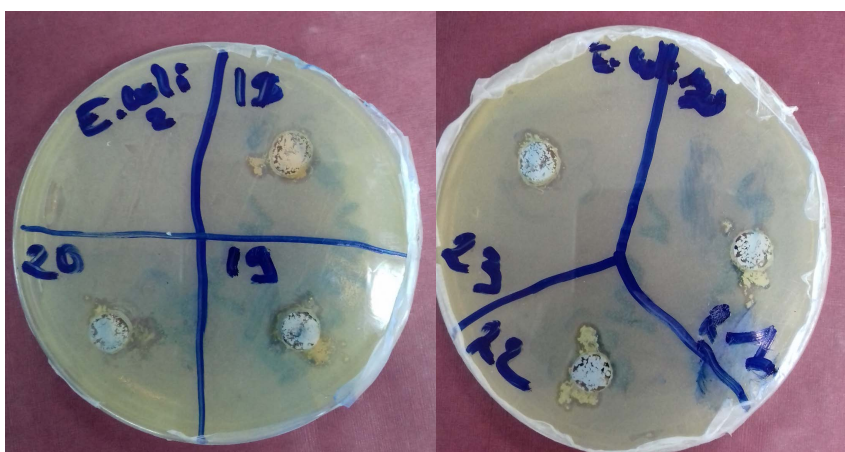


Figure 7. Antimicrobial activity of nanocomposites with *E. coli* bacterial strains, in dark.

Against gram-negative bacteria *E. coli* (Figure 7), inhibition zones are smaller than *S. aureus*. These observations could be result to the cell wall structure of bacteria. Indeed, the gram-positive bacteria have a relatively cell wall composed of many layers of peptidoglycan polymer and only one membrane (plasma membrane). The gram-negative bacteria have only a thin layer of peptidoglycan and more complex cell wall with two cell membranes, an outer membrane, and a plasma membrane. The addition of the outer membrane of the gram-negative bacteria cells influences the permeability of many molecules. The gram-negative bacteria cell wall makes difficult permeability of Ag NPs [29] [30].

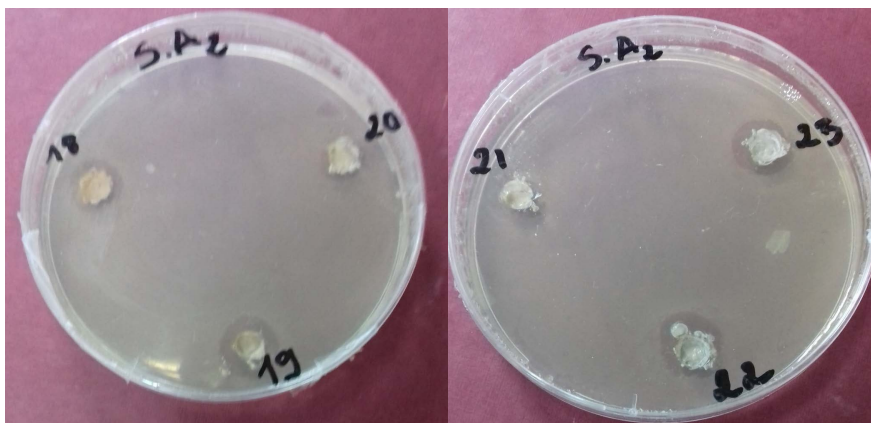
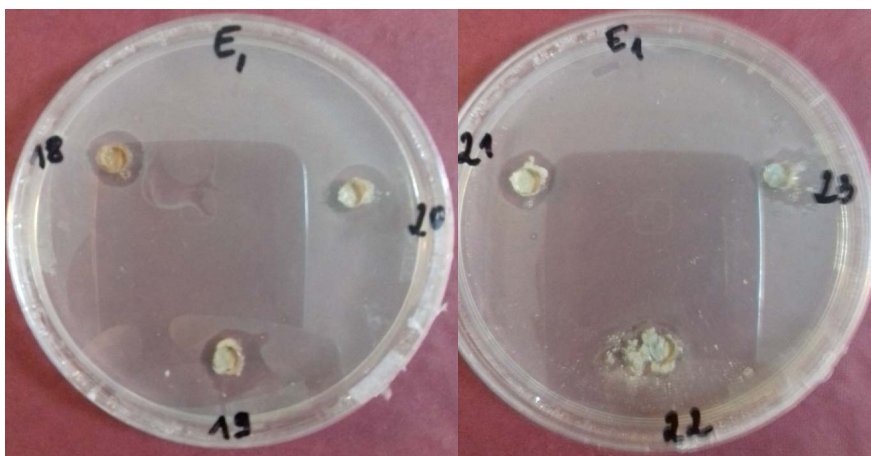
The diameter of zone of inhibition of different prepared nanocomposites is reported in Table 2. For gram-positive bacteria (*S. aureus*), the diameter of inhibition zone increase from 2 to 8 mm with growing clay loaded in the nanocomposite. For gram-negative (*E. coli*), a small increasing of 2 mm of diameter of inhibition zone was observed. These results show the synergic effect of adsorption and antimicrobial activity of Ag NPs.

3.4.2. Activity under Visible Light Irradiation

Under visible light irradiation, Figure 8 and Figure 9 show the disk diffusion

Table 2. Diameter of zone of inhibition of different prepared nanocomposites, in dark.

Samples	<i>Staphylococcus aureus</i>		<i>Escherichia coli</i>	
	Initial diameter (mm)	Final inhibition zone diameter (mm)	Initial diameter (mm)	Final inhibition zone diameter (mm)
AgTiO ₂ /Clay[1:1]	8	16 ± 1	8	10 ± 1
AgTiO ₂ /Clay[1:0.5]	8	16 ± 1	8	10 ± 1
AgTiO ₂ /Clay[1:0.1]	8	16 ± 1	8	10 ± 1
AgTiO ₂ /Clay[1:0.05]	8	14 ± 1	8	10 ± 1
AgTiO ₂ /Clay[1:0.01]	8	12 ± 1	8	10 ± 1
AgTiO ₂	8	10 ± 1	8	10 ± 1

**Figure 8.** Antimicrobial activity of nanocomposites with *S. aureus* bacterial strains, under visible light irradiation.**Figure 9.** Antimicrobial activity of nanocomposites with *E. coli* bacterial strains, under visible light irradiation.

bactericidal photographs of *S. aureus* and *E. coli*, respectively, according of nanocomposite used. After 60 min visible light exposure, the significant inhibitions zones were observed. These observations show the antimicrobial activity of different prepared nanocomposites for *E. coli* and *S. aureus*. Indeed, under visible

Table 3. Diameter of zone of inhibition of different prepared nanocomposites, under visible light.

Samples	<i>Staphylococcus aureus</i>		<i>Escherichia coli</i>	
	Initial diameter (mm)	Final inhibition zone diameter (mm)	Initial diameter (mm)	Final inhibition zone diameter (mm)
AgTiO ₂ /Clay[1:1]	8	18 ± 1	8	16 ± 1
AgTiO ₂ /Clay[1:0.5]	8	20 ± 1	8	16 ± 1
AgTiO ₂ /Clay[1:0.1]	8	18 ± 1	8	16 ± 1
AgTiO ₂ /Clay[1:0.05]	8	20 ± 1	8	16 ± 1
AgTiO ₂ /Clay[1:0.01]	8	18 ± 1	8	14 ± 1
AgTiO ₂	8	16 ± 1	8	14 ± 1

light irradiation, TiO₂ exhibits strong bactericidal activity [31]. The photo-generated holes and electrons react with water and oxygen respectively to form various reactive species such as superoxide radicals and hydroxyl radicals [32]. Silver nanoparticles are also photoactive in presence of visible light. These nanoparticles can absorb visible light due to localized surface plasmon resonance [33], that's extending their wavelength response toward the visible region, and increasing their antibacterial activity.

In **Table 3**, the diameters of zone of inhibition of different prepared nanocomposites for *S. aureus* and *E. coli*, after 1-hour visible light exposure, have been reported. The diameter of inhibition zone increases from 8 to 12 mm, for *S. aureus*. For *E. coli*, an increasing of 6 to 8 mm of diameter of inhibition zone was observed. Thus, during visible light exposure, there are three synergic effects observed on our prepared nanocomposites: the adsorption of bacteria on clay, the photochemical reaction between silver nanoparticles and bacteria adsorbed and the photocatalytic reaction of hydroxyl radicals.

4. Conclusion

AgTiO₂ nanocomposite containing different amounts of clay was synthesized by hydrothermal process and characterized by several techniques successfully. XRD analysis confirmed all the prepared samples consisting of pure anatase phase. The SEM analyses show the presence of TiO₂ and silver and the surface of nanocomposites. The photocatalysis test results showing efficiency of this nanocomposites are important when the ratio (AgTiO₂)(Clay) is 1:0.5. AgTiO₂/Clay displays good antibacterial activity for *S. aureus*, without and under visible light exposure. The diameter of inhibition zone, characteristic of antibacterial activity, increases from 2 to 8 mm in the dark, and from 8 to 12 mm under irradiation. For *E. coli*, we observed significant antibacterial activity only under visible light due to the cell wall layers of this bacterium. The AgTiO₂/Clay prepared by this route can be a promising candidate to be an excellent photocatalyst and an antimicrobial with much lower cost. The synergetic photocatalytic and antibacterial activity of samples makes them potentially applicable for wastewater treatment.

Acknowledgements

This work was financially supported by 2017 CIIT-TWAS POSTDOCTORAL FELLOWSHIP. We would also like to thank Dr. Aqif Anwar, Head of Department of Interdisciplinary Research Centre in Biomedical Materials (IRCBM), Lahore Campus.

Conflicts of Interest

The authors declare no conflicts of interest regarding the publication of this paper.

References

- [1] Ajakaye, O.G. and Ibukunoluwa, M.R. (2019) Prevalence and Risk of Malaria, Anemia and Malnutrition among Children in IDPs Camp in Edo State, Nigeria. *Parasite Epidemiology and Control*, **8**, e00127. <https://doi.org/10.1016/j.parepi.2019.e00127>
- [2] Mathur, P. and Singh, S. (2013) Multidrug Resistance in Bacteria: A Serious Patient Safety Challenge for India. *Journal of Laboratory Physicians*, **5**, 5-10. <https://doi.org/10.4103/0974-2727.115898>
- [3] Sedighi, M., Vaez, H., Moghoofei, M., Hadifar, S., Oryan, G. and Faghri, J. (2015) Molecular Detection of Metallo- β -Lactamase Gene blaVIM-1 in Imipenem-Resistant *Pseudomonas aeruginosa* Strains Isolated from Hospitalized Patients in the Hospitals of Isfahan. *Advanced Biomedical Research*, **4**, 57. <https://doi.org/10.4103/2277-9175.151872>
- [4] Rai, M., Yadav, A. and Gade, A. (2009) Silver Nanoparticles as a New Generation of Antimicrobials. *Biotechnology Advances*, **27**, 76-83. <https://doi.org/10.1016/j.biotechadv.2008.09.002>
- [5] Abate, H.K., Kidane, S.Z., Feyessa, Y.M. and Gebrehawariat, E.G. (2019) Mortality in Children with Severe Acute Malnutrition. *Clinical Nutrition ESPEN*, **33**, 98-104. <https://doi.org/10.1016/j.clnesp.2019.07.001>
- [6] Nasr, M., Tawfik, A., Ookawara, S. and Suzuki, M. (2013) Environmental and Economic Aspects of Hydrogen and Methane Production from Starch Wastewater Industry. *Journal of Water and Environment Technology*, **11**, 463-475. <https://doi.org/10.2965/jwet.2013.463>
- [7] Legrini, O., Oliveros, E. and Braun, A.M. (1993) Photochemical Processes for Water Treatment. *Chemical Reviews*, **93**, 671-698. <https://doi.org/10.1021/cr00018a003>
- [8] Schiavello, M. (1997) Heterogeneous Photocatalysis. 3rd Edition, John Wiley and Sons, Hoboken.
- [9] Vincenzo, A., Marta, L., Leonardo, P. and Javier, S. (2006) The Combination of Heterogeneous Photocatalysis with Chemical and Physical Operations: A Tool for Improving the Photoprocess Performance. *Journal of Photochemistry and Photobiology C: Photochemistry Reviews*, **7**, 127-144. <https://doi.org/10.1016/j.jphotochemrev.2006.12.001>
- [10] Huh, A.J. and Kwon, Y.J. (2011) "Nanoantibiotics": A New Paradigm for Treating Infectious Diseases Using Nanomaterials in the Antibiotics Resistant Era. *Journal of Controlled Release*, **156**, 128-145. <https://doi.org/10.1016/j.jconrel.2011.07.002>
- [11] Kim, J.S., Kuk, E., Yu, K.N., Kim, J.-H., Park, S.J., Lee, H.J., Kim, S.H., Park, Y.K., Park, Y.H. and Hwang, C.-Y. (2007) Antimicrobial Effects of Silver Nanoparticles.

- Nanomedicine: Nanotechnology, Biology and Medicine*, **3**, 95-101.
<https://doi.org/10.1016/j.nano.2006.12.001>
- [12] Tran, Q.H. and Le, A.-T. (2013) Silver Nanoparticles: Synthesis, Properties, Toxicology, Applications and Perspectives. *Advances in Natural Sciences: Nanoscience and Nanotechnology*, **4**, Article ID: 033001.
<https://doi.org/10.1088/2043-6262/4/3/033001>
- [13] Sre, P.R., Reka, M., Poovazhagi, R., Kumar, M.A. and Murugesan, K. (2015) Antibacterial and Cytotoxic Effect of Biologically Synthesized Silver Nanoparticles Using Aqueous Root Extract of *Erythrina indica* Lam. *Spectrochimica Acta Part A: Molecular and Biomolecular Spectroscopy*, **135**, 1137-1144.
<https://doi.org/10.1016/j.saa.2014.08.019>
- [14] Kong, H. and Jang, J. (2008) Antibacterial Properties of Novel Poly(methyl methacrylate) Nanofiber Containing Silver Nanoparticles. *Langmuir*, **24**, 2051-2056.
<https://doi.org/10.1021/la703085e>
- [15] Jang, B., Badger, J.C., Elasri, M.O. and Mathias, L.J. (2007) Antibacterial Fluoromicas: A Novel Delivery Medium. *Applied Clay Science*, **38**, 57-63.
<https://doi.org/10.1016/j.clay.2007.01.002>
- [16] Viana, M., Mohallem, N., Miquita, D., Balzuweit, K. and Silva-Pinto, E. (2013) Preparation of Amorphous and Crystalline Ag/TiO₂ Nanocomposite Thin Films. *Applied Surface Science*, **265**, 130-136. <https://doi.org/10.1016/j.apsusc.2012.10.151>
- [17] Sun, J., Liu, N., Zhai, S., Xiao, Z., An, Q. and Huang, D. (2014) Gold-Titania/Protanated Zeolite Nanocomposite Photocatalysts for Methyl Orange Degradation under Ultraviolet and Visible Irradiation. *Materials Science in Semiconductor Processing*, **25**, 286-293. <https://doi.org/10.1016/j.mssp.2014.01.003>
- [18] Yu, B., Leung, K.M., Guo, Q., Lau, W.M. and Yang, J. (2011) Synthesis of Ag-TiO₂ Composite Nano Thin Film for Antimicrobial Application. *Nanotechnology*, **22**, Article ID: 115603. <https://doi.org/10.1088/0957-4484/22/11/115603>
- [19] Younas, H., Qazi, I.A., Hashmi, I., Awan, M.A., Mahmood, A. and Qayyum, H.A. (2014) Visible Light Photocatalytic Water Disinfection and Its Kinetics Using Ag-Doped Titania Nanoparticles. *Environmental Science and Pollution Research*, **21**, 740-752. <https://doi.org/10.1007/s11356-013-1980-7>
- [20] Guillaume, P., Chelaru, A., Visa, M. and Lassiné, O. (2018) Titanium Oxide-Clay as Adsorbent and Photocatalysts for Wastewater Treatment. *Journal of Membrane Science & Technology*, **8**, 176-186.
- [21] García-Serrano, J., Gómez-Hernández, E., Ocampo-Fernández, M. and Pal, U. (2009) Effect of Ag Doping on the Crystallization and Phase Transition of TiO₂ Nanoparticles. *Current Applied Physics*, **9**, 1097-1105.
<https://doi.org/10.1016/j.cap.2008.12.008>
- [22] Konan, K.L., Peyratout, C., Bonnet, J.-P., Smith, A., Jacquet, A., Magnoux, P. and Ayrault, P. (2007) Surface Properties of Kaolin and Illite Suspensions in Concentrated Calcium Hydroxide Medium. *Journal of Colloid and Interface Science*, **307**, 101-108. <https://doi.org/10.1016/j.jcis.2006.10.085>
- [23] Wang, Y., Huang, Y., Ho, W., Zhang, L., Zou, Z. and Lee, S. (2009) Biomolecule-Controlled Hydrothermal Synthesis of C-N-S-Tridoped TiO₂ Nanocrystalline Photocatalysts for NO Removal under Simulated Solar Light Irradiation. *Journal of Hazardous Materials*, **169**, 77-87. <https://doi.org/10.1016/j.jhazmat.2009.03.071>
- [24] Pohan, A., Goure-Doubi, H., Kouyate, A., Nasir, M., Visa, M. and Ouattara, L. (2019) Hydrothermal Sol-Gel TiO₂ Nanoparticles Fixed to Clay and Its Photocatalytic Application for the Degradation of Methyl Orange. *Mediterranean Journal of Chemistry*, **9**, 125-132. <https://doi.org/10.13171/mjc92190918430ap>

- [25] Hsieh, C.-T., Fan, W.-S., Chen, W.-Y. and Lin, J.-Y. (2009) Adsorption and Visible-Light-Derived Photocatalytic Kinetics of Organic Dye on Co-Doped Titania Nanotubes Prepared by Hydrothermal Synthesis. *Separation and Purification Technology*, **67**, 312-318. <https://doi.org/10.1016/j.seppur.2009.03.041>
- [26] Baiju, K., Shajesh, P., Wunderlich, W., Mukundan, P., Kumar, S.R. and Warriar, K. (2007) Effect of Tantalum Addition on Anatase Phase Stability and Photoactivity of Aqueous Sol-Gel Derived Mesoporous Titania. *Journal of Molecular Catalysis A: Chemical*, **276**, 41-46. <https://doi.org/10.1016/j.molcata.2007.06.017>
- [27] Srivatsa, K., Bera, M. and Basu, A. (2008) Pure Brookite Titania Crystals with Large Surface Area Deposited by Plasma Enhanced Chemical Vapour Deposition Technique. *Thin Solid Films*, **516**, 7443-7446. <https://doi.org/10.1016/j.tsf.2008.02.002>
- [28] Rao, K.V.S., Lavédrine, B. and Boule, P. (2003) Influence of Metallic Species on TiO₂ for the Photocatalytic Degradation of Dyes and Dye Intermediates. *Journal of Photochemistry and Photobiology A: Chemistry*, **154**, 189-193. [https://doi.org/10.1016/S1010-6030\(02\)00299-X](https://doi.org/10.1016/S1010-6030(02)00299-X)
- [29] Brown, L., Wolf, J.M., Prados-Rosales, R. and Casadevall, A. (2015) Through the Wall: Extracellular Vesicles in Gram-Positive Bacteria, Mycobacteria and Fungi. *Nature Reviews Microbiology*, **13**, 620-630. <https://doi.org/10.1038/nrmicro3480>
- [30] Schatz, A., Bugle, E. and Waksman, S.A. (1944) Streptomycin, a Substance Exhibiting Antibiotic Activity against Gram-Positive and Gram-Negative Bacteria. *Proceedings of the Society for Experimental Biology and Medicine*, **55**, 66-69. <https://doi.org/10.3181/00379727-55-14461>
- [31] Fujishima, A., Rao, T.N. and Tryk, D.A. (2000) Titanium Dioxide Photocatalysis. *Journal of Photochemistry and Photobiology C: Photochemistry Reviews*, **1**, 1-21. [https://doi.org/10.1016/S1389-5567\(00\)00002-2](https://doi.org/10.1016/S1389-5567(00)00002-2)
- [32] Mills, A. and Le Hunte, S. (1997) An Overview of Semiconductor Photocatalysis. *Journal of Photochemistry and Photobiology A: Chemistry*, **108**, 1-35. [https://doi.org/10.1016/S1010-6030\(97\)00118-4](https://doi.org/10.1016/S1010-6030(97)00118-4)
- [33] Zhou, X., Liu, G., Yu, J. and Fan, W. (2012) Surface Plasmon Resonance-Mediated Photocatalysis by Noble Metal-Based Composites under Visible Light. *Journal of Materials Chemistry*, **22**, 21337-21354. <https://doi.org/10.1039/c2jm31902k>